ACS ES&T Water

pubs.acs.org/estwater

Article

Superhydrophobic Cellulosic Membranes for Membrane Distillation

Ritika Joshi, Jackie Zheng, Kai Chi, Sophie Zhang, Xiangyu Huang, Pejman Hadi, Tom Lindstrom,* and Benjamin S. Hsiao*

Cite This: *ACS EST Water* 2022, 2, 1822–1833

Read Online

ACCESS | Metrics & More | Article Recommendations | Supporting Information

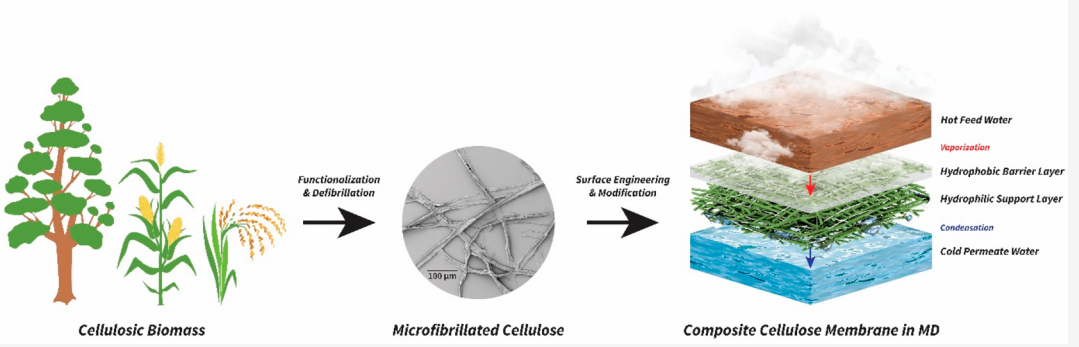

ABSTRACT: Membrane distillation (MD) offers robust drinking water solutions to off-grid global communities. However, synthetic polymer-based MD membranes often hamper this goal due to the relative high cost and nondegradable nature. In this study, we demonstrate a composite cellulosic membrane system, using neat microfibrillated cellulose (MFC) as a scaffold and its composite as a barrier layer, in which MFC can be extracted from any lignocellulose biomass source. The membranes exhibited superhydrophobicity (water contact angle >150°), high porosity, and high wet mechanical strength. The superhydrophobicity was induced by the surface microstructure of the barrier layer containing hydrophobic inorganic fillers (precipitated calcium carbonate) dispersed in a cross-linked MFC scaffold treated by a hydrophobic sizing agent. The wet strength and high porosity were achieved by the cross-linking reaction between MFC fibers, which maintained as hydrophilic but water-resistant. The best performing cellulosic membrane was tested for desalination of simulated blackish water and seawater (8 g/L NaCl solution to 35 g/L NaCl solution) using the direct contact membrane distillation (DCMD) method and exhibited high-water flux and high salt rejection ratio, comparable to the performance of commercial polytetrafluoroethylene (PTFE) membranes. The demonstrated composite cellulosic membrane system, manufactured by using typical papermaking ingredients and procedures, offers promising features that can replace synthetic polymeric membranes for sustainable MD operations.

KEYWORDS: *cellulose, microfibrillated, superhydrophobic, membrane distillation, desalination*

1. INTRODUCTION

A lack of safe, adequate, and clean water supply is one of the most pressing global problems in this century. The United Nations estimates that over 2 billion people are now living in high water stress regions.[1] The problem will get even worse in dry, arid, and coastal regions. This is because about 2.1 billion people live in drylands today, and roughly more than 200 million live along coastlines less than 5 m above the sea level.[2,3] These people can experience severe challenges to access sustainable drinking water supply due to chronical and/or acute water shortage from climate change and extreme weather events. The global pandemic of COVID-19 has further highlighted the importance of having adequate clean water in order to maintain the public health of the society. Thus, there is an urgent need to create sustainable materials and technologies that can harvest fresh water from a range of diverse sources, including seawater, brackish water, and wastewater,[4] while maintaining the environmentally friendly principles outlined in the UN's Sustainable Development Goals.[1]

For the off-grid communities in dry and arid regions with limited resources, implementing existing water desalination technologies, such as reverse osmosis and thermal distillation, can be challenging as these technologies are energy and capital intensive and have a high environmental footprint.[5] Membrane distillation (MD) offers a unique approach to overcome these challenges and can provide a sustainable drinking water

Received: July 28, 2022
Revised: August 21, 2022
Accepted: August 23, 2022
Published: September 1, 2022

solution. This is because MD requires a simple system infrastructure with a low operating pressure that can be operated by a range of alternative renewable energy sources, such as solar and geothermal energy, and even low-grade thermal energy from waste heat.[5,6] MD is a thermally driven membrane separation process, consisting of a hydrophobic porous membrane, which allows for the passage of water vapors and leaves behind nonvolatile solutes in the hotter feed solution.[7] An ideal membrane for MD operations should possess certain characteristics, such as hydrophobicity, high porosity, suitable pore size (the mean value should be in the range 0.1−1.0 μm), good mechanical strength, suitable layer thickness, and good thermal stability.[7,8] Current commercial MD membranes are mainly made of petroleum-derived polymers, such as polytetrafluoroethylene (PTFE), polyvinylidene difluoride (PVDF), and polypropylene (PP),[9−11] where the recent advance in nanofiber technology has further enhanced the flux of these membranes.[12] For example, Liao et al.[13] demonstrated a superhydrophobic Si-modified PVDF membrane fabricated by electrospinning, exhibiting superior MD performance (i.e., higher water flux) to commercial membranes. However, the above membranes based on synthetic polymeric materials are not biodegradable, where their production and disposal often pose a large carbon footprint and growing environmental concerns.[14]

To improve the sustainability of MD operation, it is of great interest to develop membranes using materials derived from natural resources, where the manufacturing method can be low cost and the membrane performance can be high but environmentally friendly. As cellulose is the most abundant renewable polymer on Earth, it is particularly desirable to explore the use of cellulose fibers as the scaffolding materials to create highly permeable MD membranes. Cellulose fibers can be extracted from any kind of lignocellulosic sources, including underutilized biomass feedstocks such as agricultural residues, recycled cellulosic products, and industrial waste.[15] These fibers have unique structural and mechanical properties and are abundant, cost-effective, and environmentally benign. They have been used primarily in the pulp, paper, and packaging industry, but functionalized cellulose fibers have recently been recognized as effective remediation materials for water purification, such as sorbent media, photocatalytic scaffolds, and water filters.[16−18]

The presence of varying hydroxyl groups on the cellulose surface allows for the implementation of versatile chemical modification schemes to introduce different functionalities on the fiber surface and/or to fibrillate the fibers into micro- or nanoscale. The common chemical treatments include carboxymethylation, TEMPO-oxidation, nitro-oxidation reactions, etc.,[19−21] which generate a negatively charged fiber surface. These charged fibers can be easily delaminated into microfibrillated cellulose (MFC) or cellulose nanofibers (CNFs), depending on the chemical pathways and subsequent mechanical treatments. These fibers are hydrophilic and can be used to create porous membranes, where the average pore size of the membrane is related to the fiber diameter.[22] However, for MD operations, the membranes must be hydrophobic to prevent the penetration of the feedwater. One major objective of the present study is to use hydrophilic microfibrillated cellulose fibers and create hydrophobic membranes with an environmentally friendly approach.

There have been several studies illustrating the creation of hydrophobic cellulosic surfaces using different approaches, such as by employing fluoropolymers or silanes as interfacial chemical agents in combination with processing methods, such as chemical vapor deposition, plasma treatment, and elecrtrospinning.[23−28] For example, Dizge et al.[26] demonstrated a superhydrophobic and oleophobic membrane by using electrospun cellulose nanofibers as a scaffolding substrate, subsequently modified by the incorporation of silica nanoparticles and chemical vapor deposition of fluoroalkylsilanes. This membrane system exhibited very high wetting resistance and a stable flux performance. Hou et al.[29] fabricated a nanowood-derived MD membrane system, also exhibiting high intrinsic vapor permeability and thermal efficiency. The nanowood membrane was made hydrophobic by the modification of perfluorodecyltriethoxysilanes (FAS) after the removal of the lignin component followed by the freeze-drying treatment. Arumugham et al.[30] demonstrated a dual-layered perfluorooctanoic acid functionalized melamine (PFOM) nanofillers embedded poly(vinylidene fluoride) casted on a cellulose substrate for direct contact membrane distillation (DCMD). The 1 wt % PFOM membrane showed a high flux and rejection ratio for simulated seawater desalination. Nassrullah et al.[31] also demonstrated a composite zeolite-cellulose functionalized polyvinylidenefluoride-*co*-hexafluoropropylene (PVH) membrane for desalination, which showed improved MD efficiency. It was apparent that the above membrane preparation procedures are not simple and often not environmentally friendly.

In this study, we demonstrate a relatively straightforward method to prepare superhydrophobic cellulose-based membranes containing a dual-layered structure: a bottom hydrophilic support layer to provide the wet mechanical strength and a top superhydrophobic barrier layer to provide the MD functionality. The basic component of this membrane system is microfibrillated cellulose (MFC) obtained by the carboxymethylation process of cellulosic biomass.[17] The manufacturing of these membranes is mainly based on typical papermaking techniques and equipment, where all additives and chemical agents are routinely used in the pulp and paper industry. Specifically, to offer wet mechanical strength and water retention capability of the support layer, MFC was cross-linked with polyamideamine-epichlorohydrin (PAE, wet strength resin in papermaking) by forming an ester bond between the azetidinium group in PAE and the carboxyl group in MFC.[32] To obtain the hydrophobicity of the barrier layer, a common additive in papermaking (precipitated calcium carbonate, PCC) was incorporated in the PAE cross-linked MFC scaffold and subsequently coated with alkyl ketene dimer (AKD, a typical sizing agent used to provide hydrophobicity in papermaking) using a dip-coating process. The composite cellulosic membrane was characterized thoroughly in terms of morphology, porosity, hydrophobicity, wet mechanical strength, and MD performance.

2. EXPERIMENTAL SECTION

2.1. Materials. Never-dried total chlorine free (TCF) bleached sulfite dissolving pulp (trade name: Dissolving Plus) from a mixture of Norway spruce (60%) and Scottish pine (40%) was obtained from Domsjö Fabriker (Aditya Birla Group, Mumbai, India), as the feedstock material. The pulp possessed a hemicellulose content of 4.5% (w/w) (measured by the solubility in 18% NaOH) and a lignin content of 0.6% (w/w). All chemicals in the carboxymethylation reaction were of ACS grade reagents and used without further purification.

https://doi.org/10.1021/acsestwater.2c00343
ACS EST Water 2022, 2, 1822−1833

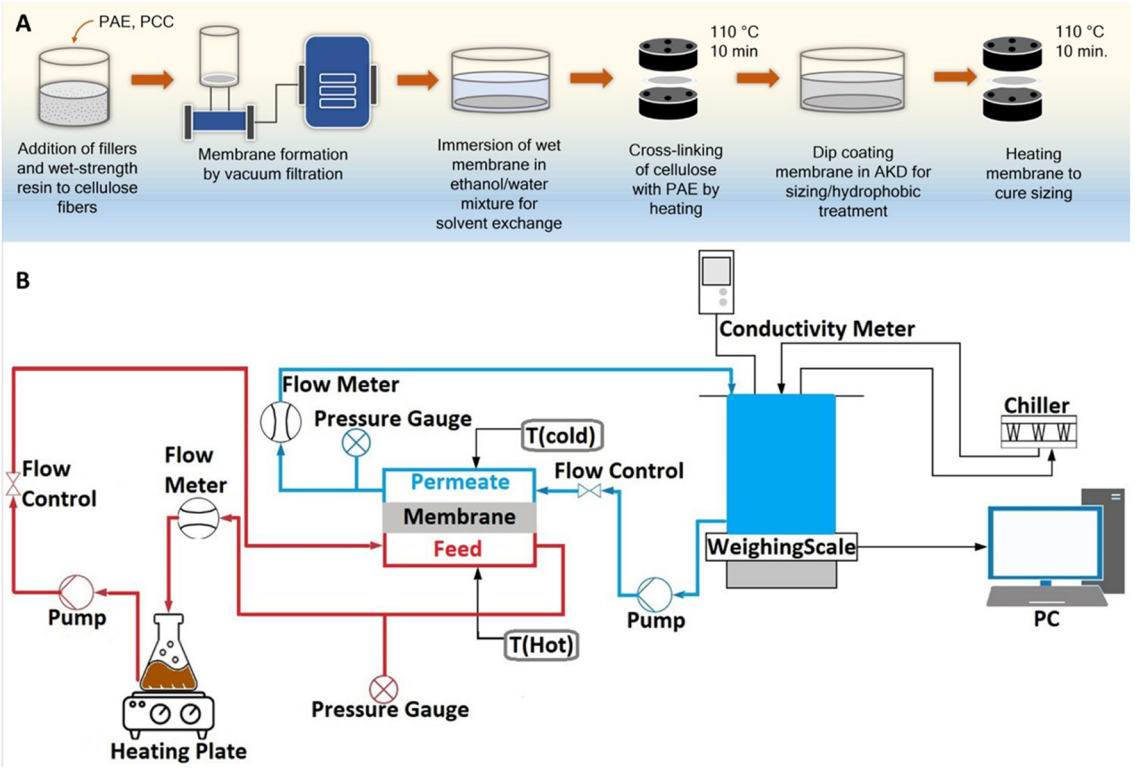

Figure 1. (A) Schematic illustration of the fabrication of the hydrophobic layer for assembly of MD composite cellulosic membranes. (B) Flow diagram of the lab-scale direct contact membrane distillation (DCMD) system.

These chemicals included monochloroacetic acid, sodium bicarbonate, ethanol, and isopropanol, and they were purchased from Fisher Scientific (Hampton, NH). Polyamide-amine epichlorohydrin (Kymene 920A) and alkyl ketene dimer emulsion (Hercon 100) were kindly provided by Solenis (Wilmington, DE). Precipitated calcium carbonate (PCC, ALBACAR HO) was provided by Specialty Minerals Inc. (New York, NY) Two types of commercial polytetrafluoro-ethylene (PTFE) membranes, PTFE015 and MSPTFE022B, were obtained from Zhejiang Kertice Hi-tech Fluor-material Co., LTD (Zhejiang, China) and Membrane Solutions (Auburn, WA), respectively.

2.2. Preparation and Characterization of Micro-fibrillated Cellulose (MFC). MFC was prepared by homogenization of cellulose microfibers after the carboxyme-thylation pretreatment[19] of pulp fibers. The details of the MFC preparation procedures and characterization results are described in the Supporting Information.

2.3. Fabrication and Characterization of Composite Cellulosic Membranes. The dual-layered composite membranes were fabricated using MFC as the scaffolding material. In these membranes, the bottom layer functioned as a hydrophilic support substrate and the top layer functioned as a hydrophobic barrier layer. A schematic representation for the top hydrophobic layer preparation is shown in Figure 1A. To fabricate this barrier layer, PAE (a wet-strength resin in papermaking) and PCC (cluster size about 1 to 4 μm) were added to a homogenized MFC aqueous dispersion and stirred for 30 min at room temperature.[33,34] The membrane was prepared using a flat vacuum filtration unit using a 0.65 μm DVPP filter (Millipore). After filtration, the wet membrane was immersed in ethanol/water (70:30) solution for solvent exchange for 1 h. The membrane was then heated at 110 °C for 10 min to initiate the cross-linking reaction.[32] The hydrophobic modification was carried out by dip-coating of cross-linked membrane in a 0.2 wt % AKD emulsion, containing sodium bicarbonate (catalyst) for 1 h.[35] The membrane was subsequently heated and cured at 110 °C for 10 min and conditioned at room temperature for 18 h. The best performing membrane contained a 1:1 PAE to MFC charge ratio and a 1:2 PCC to MFC fiber weight ratio, respectively, and had a typical mean thickness of 105 μm.

The hydrophilic support layer was prepared in a similar manner by adding PAE to MFC dispersion (1:1 charge molar ratio) followed by the solvent exchange and heating treat-ments. The average thickness of hydrophilic layer was 170 μm. The membranes were conditioned at room temperature for 24 h before characterization and testing. The composite membrane was simply prepared by physical stacking of the hydrophobic barrier layer and hydrophilic layer together.

The dual-layered composite membranes were characterized in terms of tensile strength, water retention, surface morphology, contact angle, pore-size, and porosity, and these characterization methods are described in the Supporting Information.

2.4. Membrane Distillation Evaluation of Composite Cellulosic Membranes. The performance of composite cellulosic membranes and the comparison with that of two commercial PTFE membranes were evaluated using a desalination test with a custom-built laboratory scale direct contact membrane distillation (DCMD) system (Figure 1B). The composite cellulosic membranes were inserted in a custom-made crossflow membrane cell with an effective surface area of 13.05 cm^2. Two pumps (BYT-7A015DC, Bayite) were used to circulate hot- and cold-water streams throughout the DCMD system. The flow rate was kept constant on both hot

https://doi.org/10.1021/acsestwater.2c00343
ACS EST Water 2022, 2, 1822−1833

and cold sides at 1 LPM (liters per minute). The temperature was regulated by two recirculating water streams using a digital hot plate (Isotemp Fisherbrand, Fisher Scientific) and a water chiller (1/10 HP, Ecoplus) on the hot and cold sides, respectively. The NaCl solution (8 or 35 g/L) was used as a hot feed solution and distilled water was collected and functioned as a cold permeate solution. The desalination performance was evaluated for each membrane with a hot feed temperature ranging from 40 to 60 °C, while keeping the cold permeate temperature at 20 °C. The water vapor flux across the cellulosic membrane was calculated by monitoring the weight gain on the permeate side using a digital balance (Explorer EX10201, OHAUS) connected to a computer and recorded at an interval of 5 min. The salt rejection ratio by the membrane was measured by observing the conductivity of the permeate solution using a calibrated conductivity meter (Oakton Con6+ series, Cole-Parmer) at an interval of 30 min. The salt rejection ratio was calculated using eq 1:

$$\text{salt rejection } (\%) = \frac{\text{conductivity}_{\text{feed}} - \text{conductivity}_{\text{permeate}}}{\text{conductivity}_{\text{feed}}} \quad (1)$$

3. RESULTS AND DISCUSSION

3.1. Fabrication of Superhydrophobic Cellulosic Membrane Based on Microfibrillated Cellulose. The membrane's scaffolding material MFC was prepared by homogenization of carboxymethylated cellulose microscale fibers, where the degree of fibrillation could be controlled by the mechanical processing conditions (i.e., the applied pressure and number of passes). It was found that the concentration of carboxymethylated cellulose fibers, ranging from 0.4 to 0.6 wt %, could yield the suitable fiber dimensions for the fabrication of both hydrophobic and hydrophilic layers in the composite membrane with a desired porosity and mean pore size. The MFC fibers with varying mean fiber dimensions (determined by ImageJ software) obtained by different homogenization conditions are summarized in Table 1. SEM images of the representative MFC fibers with varying size distributions are shown in Figure 2.

Table 1. Comparison of the Mean Fiber Width of MFC by Homogenization at Different Processing Conditions

fiber conc. (wt %) and no. of passes	pressure (bar)	mean fiber width (μm)
0.5 wt %, one pass	250	35.7 ± 3.8
0.6 wt %, one pass	450	23.5 ± 3.2
0.6 wt %, two pass	450	8.90 ± 2.6

In Table 1, it was found that MFC obtained by homogenization at 450−500 bar using one pass and 0.6 wt % fiber concentration yielded the most suitable fiber width distribution in scaffolding layers with the desired porosity and pore size range for MD operation. The chosen MFC possessed a mean fiber width of 23.5 ± 3.2 μm (Figure 2B,E) and a fiber length of a few hundred micrometers. In fact, MFC was a mixture of a small portion of fibrillated nanofibers and a large portion of partially fibrillated microfibers. The mean fiber width of the partially fibrillated microfibers could be estimated from the initial carboxymethylated fibers before homogenization, and it was about 40 μm (Figure 2D). The mean fiber width of the fibrillated nanofibers was determined by TEM, as detailed in the Supporting Information. TEM imaging indicated that the width of the nanofiber in MFC was in the range 10−20 nm and the fiber length ranged from a few nanometers to a few microns (Figure 2F). The dual distributions of nanofibers and partially fibrillated microfibers in the MFC dispersion provided an ideal scaffolding platform to fabricate both hydrophilic and hydrophobic layers in the composite cellulosic membranes.

Polyamideamine-epichlorohydrin (PAE) was used to cross-link the MFC scaffold in order to enhance the wet integrity of the composite cellulosic membrane. In this procedure, PAE was first incorporated into a MFC dispersion (the wet-end addition). The cast layer was subsequently heated to a high temperature (i.e., 110 °C for 10 min), where the carboxylate groups on MFC could act as anionic retention sites to react with the cationic azetidinium rings in PAE molecules (Figure S3 in the Supporting Information), resulting in the formation of covalent ester bonds.[32,36] The FTIR analysis (Figure 3A) of pure MFC and the PAE cross-linked MFC layer exhibited the difference of a spectrum peak at 1728 cm^{-1}, which could be attributed to the C═O vibration of the ester bond formed by cross-linking.[33] Additionally, the peaks at around 1640 cm^{-1} due to the C═O vibration in amide I and 1550 cm^{-1} due to the N—H stretching in amide II confirmed the presence of PAE in the cross-linked MFC scaffold.[32,37] The water retention studies (Figure 3B) of the cross-linked layers, containing varying concentrations of PAE with a resin to fiber charge ratio from 0 to 1.0, showed a sharp decrease from 400% to 140%, respectively. The formation of the water insoluble MFC network cross-linked with ester bonds effectively decreased the water absorption capability of the cellulose scaffold and prevented its wet swelling ability.[38]

The tensile strength analysis of the PAE cross-linked MFC layers showed that even a small addition of PAE resin could greatly enhance its mechanical properties in both dry and wet states. Dry and wet tensile properties of the PAE cross-linked MFC support layers in the composite cellulosic membranes are summarized in Table S1 (Supporting Information) and Figure 3D (dry and wet tensile strength). It was seen that the tensile strength in both dry and wet states generally increased with PAE concentration, which could be attributed to the increase in the cross-linking density of ester bonds. However, the increasing cross-linking density also decreased the mobility of fibers in the network.[39] This was confirmed by a slight increase in dry and wet tensile stiffness indexes, while the strain values did not show much change with the increasing PAE content. The latter could be explained by the fact that the presence of cross-linking in the scaffold could prevent the interfibrillar slippage. It was difficult to calculate the wet tensile strength of pure MFC layer (without PAE cross-linking)[40] because the water molecules acted as a plasticizer and weakened the interfibrillar bonding and the network stiffness. The introduction of covalent linkages through PAE cross-linking clearly protected the MFC network structure from the disruptive action of water molecules. The wet strain values of the PAE cross-linked MFC films also showed a notable increase, indicating the improved ductility in the wet state.

A solvent exchange procedure after the scaffold casting was used to enhance the porous structure of both barrier and support layers in the composite cellulosic membrane. This is because, for the typical membrane in MD operation, the ideal porosity should be between 30% and 80%,[7] while the drying

https://doi.org/10.1021/acsestwater.2c00343
ACS EST Water 2022, 2, 1822−1833

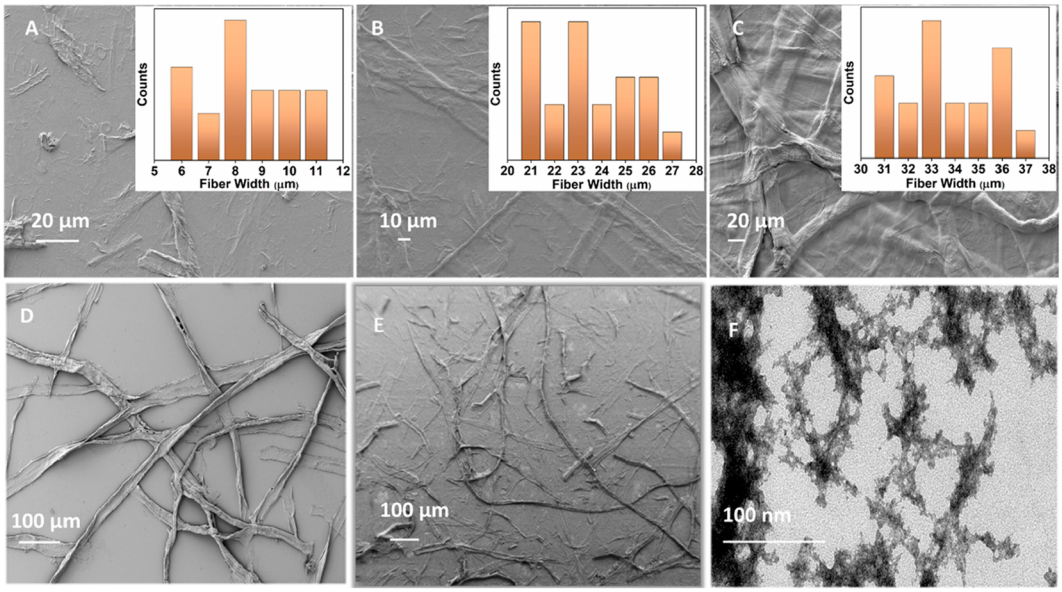

Figure 2. SEM images of partially defibrillated MFC fibers and the fiber width distribution histogram at different homogenization conditions: (A) 0.6 wt % MFC at 500 bar for two passes, (B) 0.6 wt % MFC at 450−500 bar for one pass, (C) 0.5 wt % MFC at 250 bar for one pass. (D) SEM image of carboxymethylated fibers before homogenization, (E) SEM images of partially defibrillated fibers from 0.6 WT% MFC after homogenization at 450 bar for one pass (a reduced view of (B)), and (F) TEM image of nano fragments in partially defibrillated dispersion of fibers.

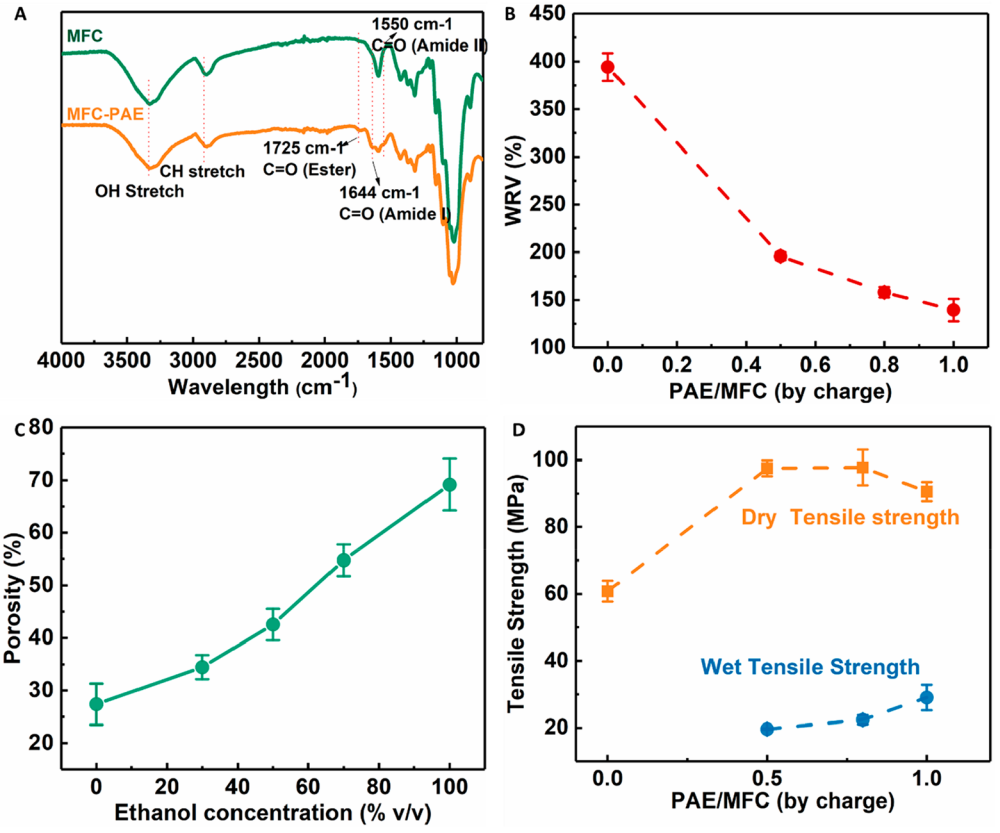

Figure 3. Characterizations of PAE cross-linked MFC films. (A) FTIR of pure MFC film without cross-linking (green) and PAE cross-linked MFC film (yellow). (B) Water retention values of cross-linked MFC films with varying PAE resin to MFC fiber charge molar ratio. (C) Porosity change of the PAE film (made with the 1:1 PAE to MFC charge molar ratio) using different ethanol concentrations. (D) Wet and dry tensile strength of cross-linked MFC membrane using varying PAE contents. The error bars represent standard deviations from three independent measurements.

process often results in a relatively low membrane porosity due to strong interfibrillar interactions between MFC fibers (due to van der Waal forces). Drying the membrane with a less polar solvent, such as ethanol (compared to water), helped to

https://doi.org/10.1021/acsestwater.2c00343
ACS EST Water 2022, 2, 1822−1833

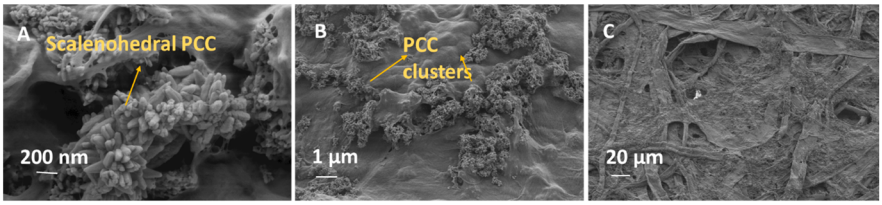

Figure 4. Dual-scale surface roughness of the hydrophobic barrier layer. SEM images showing (A) the scalenohedral shape of PCC fillers at the nanoscale; (B) PCC clusters creating microscale surface hierarchy; and (C) the enlarged view of the barrier layer surface showing the pores created by a network of interconnected fibers.

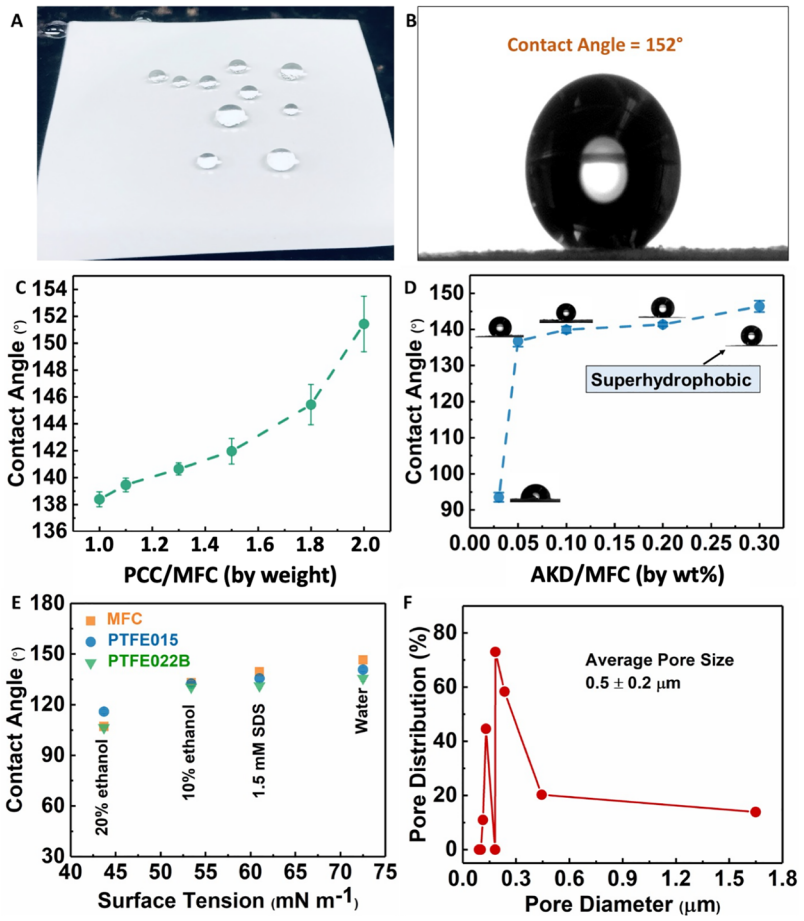

Figure 5. Hydrophobic nature of the composite cellulosic membrane. (A) Photograph of deposited water droplets on the membrane surface. (B) Water contact angle of the best performing membrane showing superhydrophobicity. (C) Contact angle as a function of the PCC content (by weight). (D) Contact angle as a function of the AKD concentration (by weight %). (E) Contact angle versus varying liquid with different surface tension for composite cellulosic membrane and two PTFE membranes (the chosen four liquids were water, sodium dodecyl sulfate (SDS), and 10% and 20% ethanol). (F) Pore size distribution of the best performing composite cellulosic membrane.

achieve a suitable porosity within the required range.[41] Figure 3C shows the change in porosity of the hydrophilic support layer (using 1:1 PAE resin to fiber charge molar ratio) using different concentrations of ethanol. It was found that the mean porosity of the PAE cross-linked MFC film increased from 27% (with no solvent exchange) to 70% (solvent exchange with 100% ethanol). The cross-linked MFC film with the mean porosity of 55% was achieved using a 70:30 ethanol/water ratio, where this film was used to prepare the hydrophobic barrier layer using the procedure outlined earlier.

Precipitated calcium carbonate (PCC) particles were incorporated into the barrier layer via wet-end addition prior to casting in order to obtain dual-scale roughness on the membrane surface.[25,42] This is because fine PCC mineral particles have been routinely used as cost-effective fillers to create hydrophobicity of cellulose fibrous products.[43] The PCC fillers used in this study were scalenohedral in shape (Figure 4A), possessing a size-distribution of clusters in the range 1−4 μm, which facilitated both micro- and submicro-scale roughness in the PAE cross-linked MFC scaffold (Figure 4B). The morphological changes in the cross-linked MFC films caused by PCC particles were evident in SEM images (Figure 4B,C), where PCC clusters adhering to nanostructured cellulose fibers were seen. The submicron size and scalenohedral shape of the PCC fillers with different spatial orientations tethered on the MFC surface enabled the

https://doi.org/10.1021/acsestwater.2c00343
ACS EST Water 2022, 2, 1822−1833

Table 2. Comparison of the Composite Cellulosic Membrane and Commercial Polymer Membranes

membrane	manufacturer	active layer	support layer	pore size (μm)	thickness (μm)	porosity (%)	contact angle (deg)	LEP (bar)[a]	ref
PP22	Osmonics Corp.	PP		0.22	150	70	138		51
QP952	Clarcor	ePTFE	PES	0.45	150−300	70−85	132		51
ECTFE	3M	ECTFE		0.43	46	67	118		51
PTFE015	Zheijiang Kertice	PTFE	PET	0.15 ± 0.1	155 ± 5	60.5 ± 4.5	139	4.52 ± 0.02	this study
PTFE022B	Membrane Solutions	PTFE	PP	0.16 ± 0.1	160 ± 10	47.3 ± 1.3	135	4.87 ± 0.07	this study
Composite MFC		hydrophobic cellulose	hydrophilic cellulose	0.50 ± 0.2	295 ± 12	55.7 ± 3.0	147	1.21 ± 0.04	this study

[a]LEP: liquid entry pressure. Pore size: the average pore size.

formation of multiscale surface hierarchical topology ideal for hydrophobation.[34] It appeared that some PCC clusters could fill the pores between the cellulose fibers and reduced the average pore size of the composite film.[44] For this reason, the wet-end addition of PCC fillers was kept as low as possible (the filler to fiber weight ratio equal to 0.5) to achieve the desired surface roughness since the high filler additions can compromise the film strength. The ζ potential of the PCC dispersion indicated that these fillers had a slightly cationic charge (7 mV). This observation confirmed the strong adhesion between positively charged PCC fillers and the negatively charged MFC scaffold due to electrostatic interaction. It was further noted that the low dosage of PCC would not exhaust the available carboxylate sites on MFC that are necessary for PAE cross-linking. The AFM images (Figure S4A−C in the Supporting Information) also showed that the surface roughness in the cross-linked MFC film containing PCC filler particles (the surface roughness R_a = 713 nm) was enhanced compared to that of the pure cross-linked MFC film without PCC (R_a = 506 nm).

Surface and internal sizing agents are commonly used in the paper industry to hydrophobize cellulose fibers.[45] In this study, alkyl ketene dimer (AKD), a common sizing agent used in papermaking, was chosen. AKD is an organic compound synthesized from fatty acids; it contains hydrophobic alkyl chains around 14−16 C atoms long. The hydrophobic treatment of PAE cross-linked MFC thin film containing PCC particles was carried out via a simple dip-coating process, where an anionic AKD emulsion in the presence of bicarbonate (0.001 M) was used. It is known that AKD can react with the carboxylate groups on cellulose and form β-ketoesters by ring opening reaction at acyl oxygen, which is the primary reaction between MFC and AKD.[35] The presence of bicarbonate can catalyze the esterification reaction between MFC and AKD by its proton donation capability.[46,47]

The contact angle measurements of hydrophobized PAE cross-linked MFC films containing PCC with different concentrations of AKD showed an increase in hydrophobicity (Figure 5D). It was seen that a contact angle of 152° was achieved for a AKD to MFC ratio of 0.2 wt %. The enhanced hydrophobic character can also be attributed to the presence of PAE molecules since cationic polyelectrolytes would act as retention aids and size accelerators for the anionic AKD emulsion.[48] The presence of a dual-scale roughness and hydrophobization by AKD of PAE cross-linked porous MFC barrier layer led to a superhydrophobic cellulosic membrane (Figure 5A and 5B). Moreover, the change in the hydrophobic characteristic by increasing the surface roughness was further explored by altering the amount of PCC (Figure 5C), where the increase in the contact angle with increasing PCC concentration highlighted the role of surface roughness in enhancing the hydrophobicity on the membrane surface. The increase in the surface roughness was also seen in the AFM image of the AKD hydrophobized barrier layer containing PCC fillers (Figure S4C in the Supporting Information). The optimized hydrophobic barrier layer showed a higher contact angle than commercial PTFE membranes (Table 2 and Figure S6 in the Supporting Information). Furthermore, the composite cellulosic membrane due to its multihierarchical structure on the barrier layer surface showed a high wetting resistance to different liquids with varying surface tension. These membrane features offer great potential of the composite cellulosic membranes for treating a wide range of contaminants in real-life wastewater. The contact angle measurements of the composite cellulosic membrane and two commercial PTFE membranes against water, 1.5 mM sodium dodecyl sulfate (SDS), and 10% and 20% ethanol are shown in Figure 5E. It was seen that the composite cellulosic membrane showed a higher wetting resistance to water, SDS, and 20% ethanol owing to the high hydrophobic character.

The top-view SEM images of the hydrophilic and hydrophobic layers are shown in Figure S5A,B (Supporting Information), respectively, whereas the cross-sectional SEM image of the composite cellulosic membrane is shown in Figure S5C (Supporting Information). It was seen that the membrane consisted of a dual-layered structure, where each layer possessed a porous network of microscale fibers deposited randomly in a nonwoven fashion. These images indicated the composite cellulosic membrane exhibited an interconnected pore structure defined by the nonwoven network, where commercial PTFE membranes exhibited a partially oriented cylindrical pore structure induced by film stretching (Figure S7 in the Supporting Information). The pore size distribution (PSD) of the composite cellulosic membrane was determined by the capillary flow porometer, where the results are shown in Figure 5F. It was seen that the average pore size of the composite cellulosic membrane was 0.5 ± 0.2 μm, which was within the targeted range of 0.1−0.6 μm to resist the wetting while maintaining the high permeate flux.[49] In contrast, the average pore size of both commercial PTFE membranes was about 0.15 μm, and their PSD was significantly narrower than that of the composite cellulosic membrane (Figure S8 in the Supporting Information). We note that the mean pore size was determined by a capillary flow porometer. In this case, the true mean pore size of the composite cellulosic membrane during MD operation may be

https://doi.org/10.1021/acsestwater.2c00343
ACS EST Water 2022, 2, 1822−1833

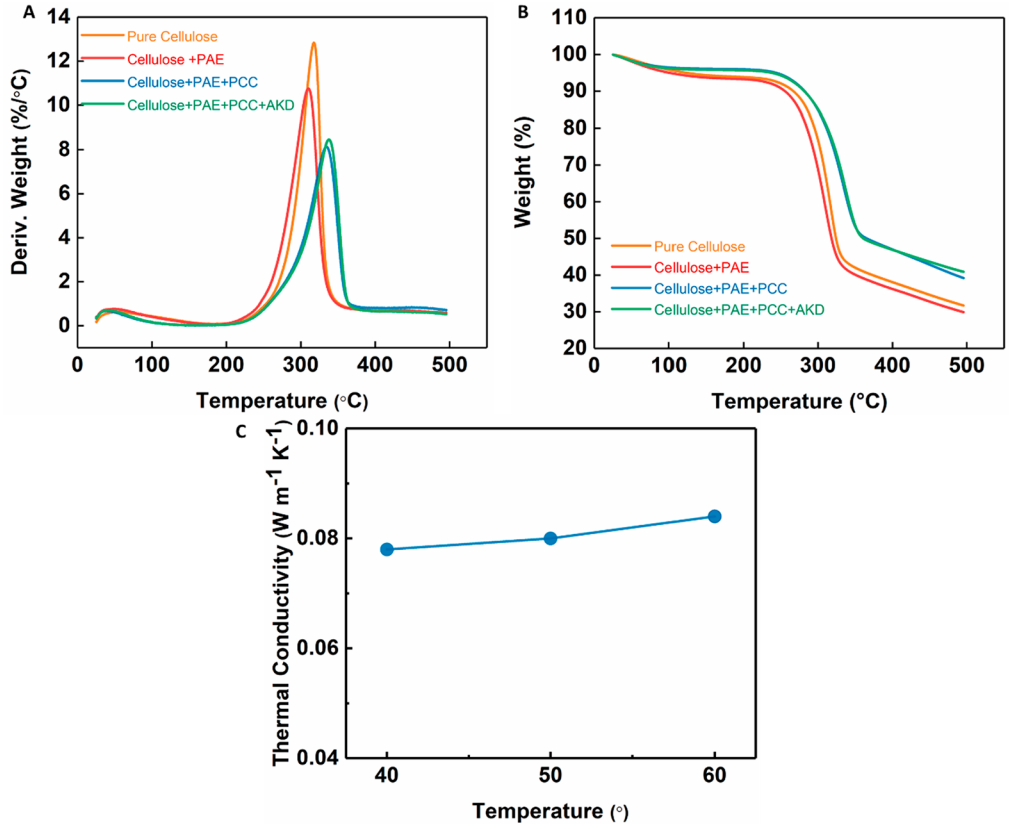

Figure 6. Thermal properties of composite cellulosic membrane. (A) Derivative thermogravimetric, (B) thermogravimetric curves for pure MFC and surface modified MFC films, and (C) thermal conductivity versus feed temperature for the composite cellulosic membrane.

smaller than 0.5 μm because MFC can swell in water. In view that the particle size distribution of PCC is in the range 1−4 μm, the possibility of PCC leaching from the cellulosic membrane during MD operation is probably low.

The best performing composite cellulosic membrane (fabricated with a 1:1 PAE to MFC charge molar ratio and a 1:2 PCC to MFC weight ratio) exhibited a decent liquid entry pressure (LEP) of 1.21 ± 0.04 bar, in spite of the relatively large average pore diameter and broad PSD, due to its superhydrophobic characteristic leading to good wetting resistance. However, the LEP of the composite cellulosic membrane was considerably lower than those of PTFE membranes (4.52 ± 0.02 bar for PTFE015 and 4.87 ± 0.07 bar for PTFE022B). This difference could be attributed to the broader pore size distribution and larger average pore size of the cellulosic membrane, as compared to narrower pore-size distribution of PTFE membranes. We believe the LEP of the composite cellulosic membrane can be further improved by using MFC with a higher degree of fibrillation, where the increase in nanofiber concentration can reduce the pore size distribution and average pore size of the composite membrane.[50]

3.2. Thermal Properties of Composite Cellulosic Membranes. The thermal conductivity of the composite cellulosic membrane was measured by a steady-state technique, where specified temperature was applied to the material (the thermal conductivity was determined by heat flux density[52]). The measurements were carried out at temperature points simulating those in MD operations. The thermal conductivity of the cellulosic membrane showed a slight increase with the increasing temperature (Figure 6C). This increase could be attributed to the anisotropic structure of the fibrous network in the membrane as well as the presence of inorganic additives used for surface modification of the membrane.[53] It was found that the measured thermal conductivity values of the cellulosic membrane are comparable to those of commercial MD membranes (i.e., thermal conductivity >0.045 W m^{-1} K^{-1}).[51] We note that the low thermal conductivity can reduce the conductive heat loss, leading to an improved flux and higher energy efficiency.[54]

The thermal degradation curves (Figure 6A) for pure MFC film, PAE cross-linked MFC film, PAE cross-linked MFC film containing PCC fillers, and cross-linked composite film with additional hydrophobic AKD sizing, all showed a two-step process. For the pure MFC film, the initial onset temperature (T_{onset}) at 249 °C and the final degradation temperature (T_{final}) at 335 °C were similar to the reported values.[55] The PAE cross-linked MFC film exhibited the improved thermal stability with a higher T_{onset} value at 252 °C, due to the conversion of some carboxylate groups into ester bonds.[38] The addition of PCC fillers and sizing agent further enhance the thermal stability of the PAE cross-linked MFC film, due to hybrid compositions and more condensed fibrous network. The DTG curves (Figure 6B) of these four samples also showed an improvement in thermal properties by wet-end additions of PAE and PCC and surface modification by AKD sequentially. The temperature at the maximum degradation rate (T_{max}) of the cross-linked MFC film after addition of PCC and PCC/AKD showed an increase in value, confirming the improvement of the thermal stability in the hydrophobic layer of the composite cellulosic membrane, which is ideal for MD operations.

https://doi.org/10.1021/acsestwater.2c00343
ACS EST Water 2022, 2, 1822−1833

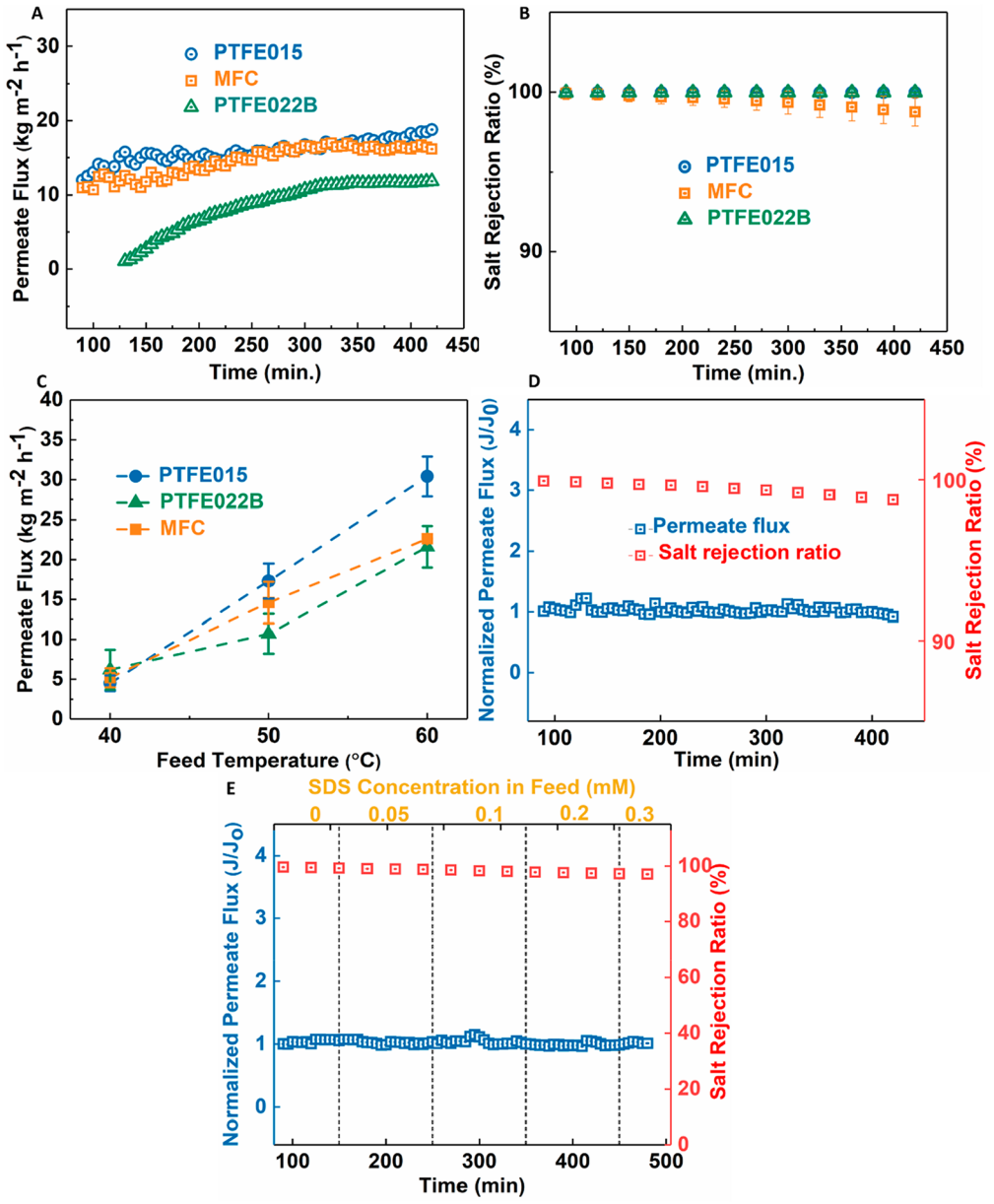

Figure 7. MD performance of composite cellulosic and commercial PTFE membranes. (A) Permeate flux and (B) salt rejection ratio of composite cellulose and commercial PTFE membranes with feed temperature at 50 °C and permeate temperature at 20 °C, where the 8 g/L NaCl solution was used as the feed solution. (C) Permeate flux versus the feed temperature for composite cellulosic and commercial PTFE membranes (8 g/L NaCl feed solution). (D) Desalination performance of the composite cellulosic membrane for simulated seawater (35 g/L NaCl solution) as the feed solution at the feed temperature of 50 °C and permeate temperature of 20 °C. (E) Normalized permeate flux (blue) and salt rejection (red) of the cellulosic membrane based on gradually increased dosage of SDS. The feed solutions contained 8 g/L NaCl and different SDS concentrations.

3.3. MD Desalination by Cellulosic Membranes and Comparison with Commercial MD Membranes. The best performing cellulosic membrane and two commercial PTFE membranes were tested for desalination using the DCMD operation (Figure 1B). First, the permeate flux and salt rejection ratio were tested using the 8 g/L NaCl feed solution (simulated brackish water) for a range of feed temperature from 40 to 60 °C. Parts A and B of Figure 7 show the permeate flux and salt rejection ratio of cellulosic and PTFE membranes using the feed temperature at 50 °C and permeate temperature at 20 °C, respectively. The average flux of the composite cellulosic membrane was 14.6 ± 2.6 kg m^{-2} $hour^{-1}$, which was close to that of PTFE015 (17.3 kg m^{-2} $hour^{-1}$) but higher than that of PTFE022B (10.7 kg m^{-2} $hour^{-1}$). The efficient performance of the composite cellulosic membrane could be attributed to its high porosity and superhydrophobicity, as the porosity of the composite membrane was ∼19% higher than that of PTFE022B (Table 2). It is known that the membrane porosity is directly proportional to the mass transfer rate of water vapor through the membrane (i.e., the permeate flux).[54]

Figure 7C illustrates the permeate flux and the feed temperature relationships for composite cellulosic and PTFE membranes using the 8 g/L NaCl feed solution. It was found that the permeate flux of all tested membranes showed an increase with the increasing feed temperature as expected. For the cellulosic membrane, the permeate flux increased from 5.2 ± 1.2 kg m^{-2} $hour^{-1}$ at 40 °C to 23.0 ± 0.06 kg m^{-2} $hour^{-1}$ at 60 °C. This is due to the increase in vapor pressure of the feed

https://doi.org/10.1021/acsestwater.2c00343
ACS EST Water 2022, 2, 1822−1833

solution, which enhances the driving force for mass (vapor) transfer.[56] When the feed solution was changed from 8 g/L NaCl solution to 35 g/L NaCl solution (simulated seawater), the flux and rejection ratio of the cellulosic membrane remained unchanged. For example, the cellulosic membrane exhibited a stable permeate flux of 10.5 ± 0.5 kg m^{-2} h^{-1}, while maintaining the high salt rejection ratio, using simulated seawater (Figure 7D).

It was interesting to note that a very slight decrease of 1.8 ± 0.8% in the salt rejection ratio with increased testing time was seen (Figure 7B,D). However, the overall salt rejection still remained above 97.5% throughout the desalination testing run. This is possibly due to the large average pore size of the composite cellulosic membrane as compared to PTFE membranes (Figure S8 in the Supporting Information).[57] If the average pore size can be reduced and the pore size distribution can be narrowed, the wetting of the cellulosic membrane can be prevented, avoiding the transition from a metastable Cassie−Baxter state to a wetted Wenzel state during the MD operation. It has been reported that, when the membrane possesses a nonuniform pore size distribution, the wetting of larger pores can occur (as the breakthrough pressure will become higher than the transmembrane pressure) while smaller pores can remain nonwetted,[58] resulting in a higher water flux but a slightly lower rejection ratio. This will be the subject of our future study to optimize the cellulose membrane structure and performance.

The desalination performance of the cellulosic membrane was also evaluated using 8 g/L NaCl feed solutions with different concentrations of SDS (Figure 7E). SDS is an anionic surfactant typically used in many cleaning and hygiene products. The presence of SDS can lower the surface tension of the feed solution, resulting in enhanced membrane wetting. With increasing SDS concentration (0.3 mM), it was seen that the composite cellulosic membrane exhibited a stable permeate flux (about 10.1 kg m^2 h^{-1}) and a high salt rejection ratio, which confirmed the efficient desalination performance of the membrane owing to its hierarchical hydrophobic surface.

We hypothesize that the dual-layered structure in the composite cellulosic membrane with the hydrophobic layer facing the hot feedwater and the hydrophilic facing the cold permeate offers some advantageous in reducing the heat polarization across the membrane in DCMD operations.[59] This feature may be further enhanced by incorporating other inorganic fillers, such as metal oxide particles and carbon black, to create superhydrophobic surface.[60] Furthermore, we report that the membrane distillation operation was performed using the composite membrane by simply stacking the hydrophilic cellulosic layer and the hydrophobic cellulosic hybrid layer together. Although the two layers can be separated after the MD operation, during the operation, the two layers seemed to adhere well, probably due to strong van der Waals force interactions and similar layer thickness.

4. CONCLUSIONS

A unique superhydrophobic composite cellulosic membrane system, consisting of a hydrophobic and hydrophilic dual-layered structure, was demonstrated by using microfibrillated cellulose as the scaffolding material. The membrane exhibited a hydrophobic surface, excellent wet mechanical strength, and suitable average pore size and pore size distribution, suitable for membrane distillation. The best performing composite cellulosic membrane displayed efficient desalination performance in the DCMD operation, catching up to the properties of commercial PTFE membranes. With the incorporation of inorganic fillers and hydrophobic sizing agent, the membrane surface exhibited a dual-scale surface structure (i.e., topology from nanoscale fiber fragments and submicroscale PCC particles), which showed higher contact angle values than those of commercial PTFE membranes against water and a variety of low surface tension liquids. The composite cellulosic membrane was prepared by fabrication practices commonly used in papermaking. The demonstrated membrane fabrication process follows a bottom-up approach utilizing the component (microfibrillated cellulose) that can be extracted from any lignocellulosic biomass plants, such as woody and nonwoody sources, including underutilized agricultural residues, weeds, and shrubs. Although the performance of demonstrated cellulose membranes is still lagging behind at the moment, they offer great potentials to complement existing commercial PTFE membranes in terms of low cost, environmental friendliness, and sustainability.

■ ASSOCIATED CONTENT

Supporting Information

The Supporting Information is available free of charge at https://pubs.acs.org/doi/10.1021/acsestwater.2c00343.

Discussions of preparation of microfibrillated cellulose, characterization of MFC, characterization of composite cellulosic membranes, and FTIR analysis of pulp and carboxymethylated fibers, figures of conductometric titration curve, FTIR spectra of pulp fibers and carboxymethylated fibers, ester bond formation between the carboxylate groups in cellulose and the azetidinium group in PAE, AFM images of PAE cross-linked MFC film, PCC filled PAE cross-linked MFC film, and AKD sized PAE-cross-linked MFC film containing PCC fillers, SEM images of top hydrophobic barrier layer and bottom hydrophilic support layer, cross-sectional view SEM image of the composite cellulosic membrane, contact angle values of two commercial PTFE membranes, SEM images showing the surface morphology of PTFE015 and PTFE022B membranes, cross-section morphology of PTFE015 and PTFE022B membranes, pore size distribution of PTFE015 (with PET support) PTFE022B (with PP support) membranes, and permeate flux and salt rejection, and tables of dry and wet tensile properties of the PAE cross-linked MFC support layers and MD performance of MFC and PTFE for desalination of brackish feed water (PDF)

■ AUTHOR INFORMATION

Corresponding Authors

Tom Lindstrom − *Department of Chemistry, Stony Brook University, Stony Brook, New York 11794, United States*; Phone: +46-70-6570194; Email: toml@kth.se

Benjamin S. Hsiao − *Department of Chemistry, Stony Brook University, Stony Brook, New York 11794, United States*; orcid.org/0000-0002-3180-1826; Phone: +1-631-632-7793; Email: benjamin.hsiao@stonybrook.edu

Authors

Ritika Joshi − *Department of Chemistry, Stony Brook University, Stony Brook, New York 11794, United States*

https://doi.org/10.1021/acsestwater.2c00343
ACS EST Water 2022, 2, 1822−1833

Jackie Zheng − *Department of Chemistry, Stony Brook University, Stony Brook, New York 11794, United States*
Kai Chi − *Department of Chemistry and Center for Integrated Electric Energy Systems, Stony Brook University, Stony Brook, New York 11794, United States;* orcid.org/0000-0003-3396-8061
Sophie Zhang − *High Technology High School, Lincroft, New Jersey 07733, United States*
Xiangyu Huang − *Department of Chemistry, Stony Brook University, Stony Brook, New York 11794, United States;* orcid.org/0000-0002-3363-3950
Pejman Hadi − *Department of Chemistry, Stony Brook University, Stony Brook, New York 11794, United States*

Complete contact information is available at: https://pubs.acs.org/10.1021/acsestwater.2c00343

Notes

The authors declare no competing financial interest.

■ ACKNOWLEDGMENTS

B.S.H. acknowledges the financial support by the Polymer Program, Division of Materials Science of the US National Science Foundation (DMR-2216585). The authors would also like to thank the Advanced Energy Research and Technology Center (AERTC) and Central Microscopy Imaging Center (CMIC) at Stony Brook University for SEM, DMA, and TEM measurements.

■ REFERENCES

(1) United Nations International Decade for Action 'Water for Life' 2005−2015. https://www.un.org/waterforlifedecade/ (accessed 2020-10-10).
(2) United Nations Decade for Deserts and The Fight Against Desertification. https://www.un.org/en/events/desertification_decade/whynow.shtml (accessed 2021-03-21).
(3) World Ocean Review. https://worldoceanreview.com/en/wor-1/coasts/living-in-coastal-areas/ (accessed 2021-03-25).
(4) Elimelech, M.; Phillip, W. A. The future of seawater desalination: Energy, technology, and the environment. *Science* **2011**, *333* (6043), 712−717.
(5) Deshmukh, A.; Boo, C.; Karanikola, V.; Lin, S.; Straub, A. P.; Tong, T.; Warsinger, D. M.; Elimelech, M. Membrane distillation at the water-energy nexus: limits, opportunities, and challenges. *Energy Environ. Sci.* **2018**, *11* (5), 1177−1196.
(6) Dongare, P. D.; Alabastri, A.; Pedersen, S.; Zodrow, K. R.; Hogan, N. J.; Neumann, O.; Wu, J.; Wang, T.; Deshmukh, A.; Elimelech, M.; Li, Q.; Nordlander, P.; Halas, N. J. Nanophotonics-enabled solar membrane distillation for off-grid water purification. *Proc. Natl. Acad. Sci. U. S. A.* **2017**, *114* (27), 6936−6941.
(7) Alkhudhiri, A.; Darwish, N.; Hilal, N. Membrane distillation: A comprehensive review. *Desalination* **2012**, *287*, 2−18.
(8) Eykens, L.; De Sitter, K.; Dotremont, C.; Pinoy, L.; Van der Bruggen, B. How to optimize the membrane properties for membrane distillation: a review. *Ind. Eng. Chem. Res.* **2016**, *55* (35), 9333−9343.
(9) Wang, P.; Chung, T.-S. Recent advances in membrane distillation processes: membrane development, configuration design and application exploring. *J. Membr. Sci.* **2015**, *474*, 39−56.
(10) Ke, H.; Feldman, E.; Guzman, P.; Cole, J.; Wei, Q.; Chu, B.; Alkhudhiri, A.; Alrasheed, R.; Hsiao, B. S. Electrospun polystyrene nanofibrous membranes for direct contact membrane distillation. *J. Membr. Sci.* **2016**, *515*, 86−97.
(11) Adnan, S.; Hoang, M.; Wang, H.; Xie, Z. Commercial PTFE membranes for membrane distillation application: Effect of microstructure and support material. *Desalination* **2012**, *284*, 297−308.
(12) Zhong, L.; Wang, Y.; Liu, D.; Zhu, Z.; Wang, W. Recent advances in membrane distillation using electrospun membranes: advantages, challenges, and outlook. *Environ. Sci.: Water Res. Technol.* **2021**, *7* (6), 1002−1019.
(13) Liao, Y.; Wang, R.; Fane, A. G. Fabrication of bioinspired composite nanofiber membranes with robust superhydrophobicity for direct contact membrane distillation. *Environ. Sci. Technol.* **2014**, *48*, 6335−6341.
(14) Lucas, N.; Bienaime, C.; Belloy, C.; Queneudec, M.; Silvestre, F.; Nava-Saucedo, J. E. Polymer biodegradation: mechanisms and estimation techniques. *Chemosphere* **2008**, *73* (4), 429−42.
(15) Klemm, D.; Kramer, F.; Moritz, S.; Lindstrom, T.; Ankerfors, M.; Gray, D.; Dorris, A. Nanocelluloses: a new family of nature-based materials. *Angew. Chem., Int. Ed. Engl.* **2011**, *50* (24), 5438−66.
(16) Huang, X.; Dognani, G.; Hadi, P.; Yang, M.; Job, A. E.; Hsiao, B. S. Cationic dialdehyde nanocellulose from sugarcane bagasse for efficient chromium(VI) removal. *ACS Sustainable Chem. Eng.* **2020**, *8* (12), 4734−4744.
(17) Wei, H.; Rodriguez, K.; Renneckar, S.; Vikesland, P. J. Environmental science and engineering applications of nanocellulose-based nanocomposites. *Environ. Sci.: Nano* **2014**, *1* (4), 302−316.
(18) Ma, H.; Burger, C.; Hsiao, B. S.; Chu, B. Nanofibrous microfiltration membrane based on cellulose nanowhiskers. *Biomacromolecules* **2012**, *13* (1), 180−6.
(19) Wagberg, L.; Decher, G.; Norgren, M.; Lindstrom, T.; Ankerfors, M.; Axnas, K. The build-up of polyelectrolyte multilayers of microfibrillated cellulose and cationic polyelectrolytes. *Langmuir* **2008**, *24*, 784−795.
(20) Isogai, A.; Saito, T.; Fukuzumi, H. TEMPO-oxidized cellulose nanofibers. *Nanoscale* **2011**, *3* (1), 71−85.
(21) Sharma, P. R.; Joshi, R.; Sharma, S. K.; Hsiao, B. S. A simple approach to prepare carboxycellulose nanofibers from untreated biomass. *Biomacromolecules* **2017**, *18* (8), 2333−2342.
(22) Sharma, P. R.; Sharma, S. K.; Lindström, T.; Hsiao, B. S. Nanocellulose-enabled membranes for water purification: perspectives. *Advanced Sustainable Systems* **2020**, *4* (5), 1900114.
(23) Song, J.; Rojas, O. Approaching super-hydrophobicity from cellulosic materials: A Review. *Nordic Pulp and Paper Research Journal* **2013**, *28*, 216−238.
(24) Huang, J.; Lyu, S.; Fu, F.; Chang, H.; Wang, S. Preparation of superhydrophobic coating with excellent abrasion resistance and durability using nanofibrillated cellulose. *RSC Adv.* **2016**, *6* (108), 106194−106200.
(25) Teisala, H.; Tuominen, M.; Kuusipalo, J. Superhydrophobic coatings on cellulose-based materials: Fabrication, properties, and applications. *Advanced Materials Interfaces* **2014**, *1*, 1300026.
(26) Dizge, N.; Shaulsky, E.; Karanikola, V. Electrospun cellulose nanofibers for superhydrophobic and oleophobic membranes. *J. Membr. Sci.* **2019**, *590*, 117271.
(27) Rana, A. K.; Gupta, V. K.; Saini, A. K.; Voicu, S. I.; Abdellattifaand, M. H.; Thakur, V. K. Water desalination using nanocelluloses/cellulose derivatives based membranes for sustainable future. *Desalination* **2021**, *520*, 115359.
(28) Leitch, M. E.; Li, C.; Ikkala, O.; Mauter, M. S.; Lowry, G. V. Bacterial nanocellulose aerogel membranes: novel high-porosity materials for membrane distillation. *Environ. Sci. Technol. Lett.* **2016**, *3* (3), 85−91.
(29) Hou, D.; Li, T.; Chen, X.; He, S.; Dai, J.; Mofid, S. A.; Hou, D.; Iddya, A.; Jassby, D.; Yang, R.; Hu, L.; Ren, Z. J. Hydrophobic nanostructured wood membrane for thermally efficient distillation. *Sci. Adv.* **2019**, *5* (8), eaaw3203.
(30) Arumugham, T.; Kaleekkal, N. J.; Rana, D.; Sathiyanarayanan, K. I. PFOM fillers embedded PVDF/cellulose dual-layered membranes with hydrophobic−hydrophilic channels for desalination via direct contact membrane distillation process. *RSC Adv.* **2019**, *9* (71), 41462−41474.
(31) Nassrullah, H.; Makanjuola, O.; Janajreh, I.; AlMarzooqi, F. A.; Hashaikeh, R. Incorporation of nanosized LTL zeolites in dual-layered PVDF-HFP/cellulose membrane for enhanced membrane distillation performance. *J. Membr. Sci.* **2020**, *611*, 118298.

(32) Obokata, T.; Isogai, A. The mechanism of wet-strength development of cellulose sheets prepared with polyamideamine-epichlorohydrin (PAE) resin. *Colloids Surf., A* **2007**, *302* (1−3), 525−531.
(33) Sharma, S.; Deng, Y. Dual mechanism of dry strength improvement of cellulose nanofibril films by polyamide-epichlorohydrin resin cross-linking. *Ind. Eng. Chem. Res.* **2016**, *55* (44), 11467−11474.
(34) Arbatan, T.; Zhang, L.; Fang, X.-Y.; Shen, W. Cellulose nanofibers as binder for fabrication of superhydrophobic paper. *Chem. Eng. J.* **2012**, *210*, 74−79.
(35) Lindström, T.; Larsson, P. T. Alkyl Ketene Dimer (AKD) sizing-a review. *Nordic Pulp & Paper Res. Journal* **2008**, *23* (2), 202−209.
(36) Obokata, T.; Yanagisawa, M.; Isogai, A. Characterization of polyamideamine-epichlorohydrin (PAE) resin: Roles of azetidinium groups and molecular mass of PAE in wet strength development of paper prepared with PAE. *J. Appl. Polym. Sci.* **2005**, *97* (6), 2249−2255.
(37) Zhang, W.; Zhang, Y.; Lu, C.; Deng, Y. Aerogels from crosslinked cellulose nano/micro-fibrils and their fast shape recovery property in water. *J. Mater. Chem.* **2012**, *22* (23), 11642.
(38) Yang, W.; Bian, H.; Jiao, L.; Wu, W.; Deng, Y.; Dai, H. High wet-strength, thermally stable and transparent TEMPO-oxidized cellulose nanofibril film via cross-linking with poly-amide epichlorohydrin resin. *RSC Adv.* **2017**, *7* (50), 31567−31573.
(39) Liang, L.; Bhagia, S.; Li, M.; Huang, C.; Ragauskas, A. J. Cross-linked nanocellulosic materials and their applications. *ChemSusChem* **2020**, *13* (1), 78−87.
(40) Benitez, A. J.; Torres-Rendon, J.; Poutanen, M.; Walther, A. Humidity and multiscale structure govern mechanical properties and deformation modes in films of native cellulose nanofibrils. *Biomacromolecules* **2013**, *14* (12), 4497−506.
(41) Henriksson, M.; Berglund, L. A.; Isaksson, P.; Lindström, T.; Nishino, T. Cellulose nanopaper of high toughness. *Biomacromolecules* **2008**, *9*, 1579−1585.
(42) Su, Y.; Ji, B.; Zhang, K.; Gao, H.; Huang, Y.; Hwang, K. Nano to micro structural hierarchy is crucial for stable superhydrophobic and water-repellent surfaces. *Langmuir* **2010**, *26* (7), 4984−9.
(43) Hu, Z.; Zen, X.; Gong, J.; Deng, Y. Water resistance improvement of paper by superhydrophobic modification with microsized CaCO3 and fatty acid coating. *Colloids Surf., A* **2009**, *351* (1−3), 65−70.
(44) Yu, X.; Bian, P.; Xue, Y.; Qian, X.; Yu, H.; Chen, W.; Hu, X.; Wang, P.; Wu, D.; Duan, Q.; Li, L.; Shen, J.; Ni, Y. Combination of microsized mineral particles and rosin as a basis for converting cellulosic fibers into ″sticky″ superhydrophobic paper. *Carbohydr. Polym.* **2017**, *174*, 95−102.
(45) Hubbe, M. Paper's resistance to wetting-A review of internal sizing chemicals and their effects. *Bioresources* **2006**, *2* (1), 106−145.
(46) Lindström, T.; Söderberg, G. On the mechanism of sizing with alkylketene dimers. Part IV. The effects of HCO3-ions and polymeric reaction accelerators on the rate of reaction between alkylketene dimers and cellulose. *Nordic Pulp & Paper Res. Journal* **1986**, *1* (2), 39−45.
(47) Lindström, T.; Glad-Nordmark, G. A study of AKD-size retention, reaction and sizing efficiency. Part 4: The effects of pH, bicarbonate and metal ions on AKD-hydrolysis. *Nordic Pulp & Paper Res. Journal* **2007**, *22* (2), 167−171.
(48) Johansson, E.; Lindström, T. A study on AKD-size retention, reaction and sizing efficiency Part 2: The effects of electrolytes, retention aids, shear forces and mode of addition on AKD-sizing using anionic and cationic AKD-dispersions. *Nordic Pulp & Paper Res. Journal* **2004**, *19* (3), 336−344.
(49) Zare, S.; Kargari, A. Membrane properties in membrane distillation. In *Emerging Technologies for Sustainable Desalination Handbook*; Gude, V. G., Ed.; Butterworth-Heinemann, 2018; pp 107−156.
(50) Lindström, T.; Aulin, C.; Naderi, A.; Ankerfors, M. *Encyclopedia of Polymer Science and Technology.* **2014**, 1−34.
(51) Vanneste, J.; Bush, J. A.; Hickenbottom, K. L.; Marks, C. A.; Jassby, D.; Turchi, C. S.; Cath, T. Y. Novel thermal efficiency-based model for determination of thermal conductivity of membrane distillation membranes. *J. Membr. Sci.* **2018**, *548*, 298−308.
(52) Uetani, K.; Hatori, K. Thermal conductivity analysis and applications of nanocellulose materials. *Sci. Technol. Adv. Mater.* **2017**, *18* (1), 877−892.
(53) Apostolopoulou-Kalkavoura, V.; Munier, P.; Bergström, L. Thermally insulating nanocellulose-based materials. *Adv. Mater.* **2021**, *33* (28), 2001839.
(54) Eykens, L.; De Sitter, K.; Dotremont, C.; Pinoy, L.; Van der Bruggen, B. Membrane synthesis for membrane distillation: A review. *Sep. Purif. Technol.* **2017**, *182*, 36−51.
(55) Ikhuoria, E. U.; Omorogbe, S. O.; Agbonlahor, O. G.; Iyare, N. O.; Pillai, S.; Aigbodion, A. I. Spectral analysis of the chemical structure of carboxymethylated cellulose produced by green synthesis from coir fibre. *Cienc. Tecnol. Mater.* **2017**, *29* (2), 55−62.
(56) El-Bourawi, M. S.; Ding, Z.; Ma, R.; Khayet, M. A framework for better understanding membrane distillation separation process. *J. Membr. Sci.* **2006**, *285* (1−2), 4−29.
(57) Ashoor, B. B.; Mansour, S.; Giwa, A.; Dufour, V.; Hasan, S. W. Principles and applications of direct contact membrane distillation (DCMD): A comprehensive review. *Desalination* **2016**, *398*, 222−246.
(58) Wang, W.; Du, X.; Vahabi, H.; Zhao, S.; Yin, Y.; Kota, A. K.; Tong, T. Trade-off in membrane distillation with monolithic omniphobic membranes. *Nat. Commun.* **2019**, *10* (1), 3220.
(59) Camacho, L.; Dumée, L.; Zhang, J.; Li, J.-d.; Duke, M.; Gomez, J.; Gray, S. Advances in membrane distillation for water desalination and purification applications. *Water* **2013**, *5* (1), 94−196.
(60) Wang, Z.; Elimelech, M.; Lin, S. Environmental applications of interfacial materials with special wettability. *Environ. Sci. Technol.* **2016**, *50* (5), 2132−50.

https://doi.org/10.1021/acsestwater.2c00343
ACS EST Water 2022, 2, 1822−1833